….

ANALYSIS OF THE SPECTRAL PROPERTIES OF FREE ELECTRON LASERS IN X-RAY AND OTHER BANDS

K.Zhukovsky[1]

Department of Theoretical Physics, Faculty of Physics, M.V.Lomonosov Moscow State University, Moscow 119991, Russia.

E-mail: zhukovsk@physics.msu.ru ; phone: +7(495)9393177

Abstract

Analytical formalism for the description of free electron laser (FEL) spectrum is proposed with account for the electron beam size, divergences, and beam energy spread and off the axis deviation in the undulators, the periodic harmonic and non-periodic constant magnetic field components in undulators. The exact analytical expressions for the spontaneous undulator radiation (UR) are obtained in terms of generalized Bessel and Airy functions, which describe the spectrum line shape and intensities. The obtained analytical formulae distinguish contributions of each installation and beam parameter in the FEL harmonic radiation. The enhanced phenomenological model is employed for the FEL modeling; it describes the harmonic powers evolution along the undulators and gradual saturation around the saturation length with account for the saturated powers oscillations. With its help we study the generation of FEL harmonics, including even, in several instances of FEL experiments LCLS, LEUTL and PAL-XFEL. We analytically demonstrate the difference in the origins of harmonics in different FELs: strong second harmonic in the LCLS experiment is caused by the deviation of the electron trajectories off the axis in 15 μm on one gain length ~1.6 m; in the LEUTL experiments it appears due to the interaction of the wide beam and the photon pulse at the gain lengths ~0.7 m. The spectrum line split due to the beam size is demonstrated analytically and compared with experimentally measured values. PAL-XFEL experiment is analyzed and compared with LCLS experiment; possibility of high harmonic radiation in it is explored. The modeling results fully agree with the measured values. The analytical formalism shows physical background for each harmonic in every FEL. It allows the analysis of the radiation and beam alignment in projected, built and working FELs and it can help minimizing losses and correcting magnetic fields and projecting experiments with FELs.

Keywords: *undulator radiation, harmonic generation, free-electron laser, off-axis effects.*

1. Introduction

The radiation of charges in spatially periodic magnetic field — the undulator radiation (UR) — was first addressed by Ginzburg [1], who also proposed that possible coherent radiation source could be based on undulators. The realization of the undulator and first UR observation was done by Motz [2]. Nowadays the UR continues to attract researcher's attention due to the latest development in the field — free electron lasers (FELs), working in X-ray band. The coherent radiation in these devices is generated by high-density electron current in precision-made long undulators, where the radiation groups electrons in micro bunches around the nods of the electromagnetic wave. The coherent radiation can be generated at the wavelengths of nanometers and less [3]–[9] in X-ray band, where the synchrotron radiation (SR) was the strongest incoherent source till recent times [10]–[13]. The coherent radiation opens new horizons for research and study of fast processes on nanoscale. Its generation in FELs requires high currents of high-energy electrons with high values of the relativistic factor $\gamma \approx 10^3 \div 10^4 >> 1$, high quality of the installations and undulators, beams with low emittances and low energy spread, and the magnetic fields close to ideally periodic. Moreover, the deviation of the electrons from the undulator axis should be kept small, in some cases ~5μm, within the size of the beams, ~20μm or so. In reality there is always some energy spread and emittance in final sized beams, the diffraction, the external magnetic fields, which are carefully evaluated and possibly compensated or screened out, and other factors, which can disrupt the coherence of electron oscillations in undulators and ruin the electron's grouping in a FEL. Moreover, there can

be the undulator field harmonics present together with the non-periodic magnetic components [14]–[19], which make the problem even more complex and hard to address with exact solutions.

Experimentally measured FEL radiation spectrums usually contain harmonics. Their power can reach ~10^{-4}÷10^{-2} of the fundamental tone power, dependently on the harmonic number; even harmonics also were registered on the axis (see, for example, [20]–[24] etc.). Intense generation of FEL harmonics can help reducing installation size and costs [25]–[28], if used instead of the fundamental tone at the same wavelength. Moreover, specially designed FELs with phase shifters were proposed [29], [30] to let high harmonics reach their natural saturation power, which is otherwise limited by the FEL-induced energy spread due to the saturation of the fundamental tone. Another approach is that of the FELs with high gain harmonic generation (HGHG) [31], [32] and cascaded undulators, where the latter are tuned on high harmonics of preceding sections. The studies (see, for example, [31]–[35]) demonstrate that short-wave radiation can be produced in more compact devices as compared with the traditional X-FEL, where the fundamental tone is generated in the undulators with the lengths up to 100 m; the whole installation has kilometric scale to be able to accelerate the electrons to high energies E~10GeV [20], [36].

In all cases the FEL harmonic radiation study is important. This problem is nontrivial due to big number of equations, which involve the moving charges and their interactions with the electromagnetic field. It is usually addressed numerically. The time dependence in numerical simulations is addressed by many temporal slices and field slices. The photon radiation field in a FEL slips ahead with respect to the electrons at one wavelength per one undulator period. To trace the slippage at shorter intervals than the undulator period, the optical field advance is interpolated between adjacent temporal slices based on this slippage rate. The number of the equations can reach $N_{eq} = N_{slice}\left(6N_e + 2\left(N_{mod} + N_{harm}\right)\right)$ [37], where N_{slice} is the number of slices in the simulation, N_e is the number of electrons in the slice, N_{mod} is the number of Gaussian optical modes for all harmonics, N_{harm} is the number of harmonics. Typical values are N_{mod}~N_{slice}~20÷30, N_e~10^4, but significantly more particles can be needed for precise simulation of the FEL harmonics [37]. Numerical 3D simulations include many parameters of the beam and the installation and allow precise computation of the FEL and radiation properties (see, for example, [38]), but they require prepared personnel and computational resources. However, even the results of complex numerical simulations can differ from each other, dependently on the program codes; the discrepancy with real FELs can be seen in any experiment. In particular, this regards the harmonic radiation, where theoretical estimations and experimental results often match less well as they do for the fundamental tone. Moreover, numerical simulations hardly evidence the reasons for the particular harmonic behaviour in specific FELs. That motivates us for the analytical study of the harmonic generation in real beams with account for the main characteristics of the FELs. Despite such study can not be exact since this would involve the solution of huge number of complex equations, it can be accurate and catch main features of the radiation in each case by accounting properly for the undulator, FEL and beam parameters. This will be done by means of generalized Bessel and Airy functions, which describe the spontaneous UR and the phenomenological FEL model, calibrated with FEL experiments [15]–[17] and numerical simulations [40], [41]. In what follows we will study the harmonic generation in several FELs, operating from visible to X-ray range, and we will figure out different and installation dependent reasons for the harmonic spectrums, including even harmonic on the axes of the considered FELs.

2. Analytical account for the UR in real beams and undulators

The UR analysis involves the study of the Bessel coefficients, which account for the parameters of the undulator and of the beam. Most of the undulators in modern FELs are planar, i.e. they have the spatially periodic magnetic field in one plane. The model of the ideally sinusoidal single-coordinate field must be complemented by the account for the field harmonics, the non-periodic magnetic components and field distortions to satisfy Maxwell equations in the finite sized beam, the account for the initial off-axis position of the electrons, the beam divergences, the electron energy spread etc. Consider first the following simplified model of the planar bi-harmonic undulator with the axis along z:

$$\vec{H} = H_0\left(\rho, \kappa + \sin(2\pi z/\lambda_u) + d\sin(2\pi h z/\lambda_u), 0\right),\ h \in \mathrm{Z},\ d, h, \rho, \kappa = \mathrm{const}, \qquad (1)$$

where λ_u is the main undulator period, H_0 is the amplitude of the main periodic undulator field, dH_0 is the amplitude of the field harmonic, ρ, κ are the factors for the possible constant field components. The additional hyperbolic components of the field in x- and y- polarizations, needed to comply with the Max-

well equations for the electron in the initial off the axis position, will be considered in what follows. The resonances λ_n of the UR with account for the off-axis deviation in the angle θ in the undulator field (1) can be written in the following usual form:

$$\lambda_n = \frac{\lambda_u}{2n\gamma^2}\left(1+\frac{k_{eff}^2}{2}+(\gamma\Theta)^2\right), \tag{2}$$

where n is the UR harmonic number, $k_{eff}^2 = k^2\varpi$, $k = H_0\lambda_u e/2\pi mc^2$ is the undulator parameter, e is the electron charge value, m is the electron mass, c is the speed of light, $\varpi = 1+(d/h)^2$, Θ is the comprehensive off-axis angle, $\Theta^2 = \theta^2+\theta_H^2-\sqrt{3}\theta_H\theta\dfrac{\rho\sin\varphi-\kappa\cos\varphi}{\sqrt{\kappa^2+\rho^2}}$, which involves besides the off-axis angle θ and around-axis angle φ also the bending angle θ_H, induced by the magnetic components $H_x = \rho H_0$, $H_y = \kappa H_0$ [42]–[45]:

$$\theta_H = \frac{2\pi}{\sqrt{3}}\frac{k}{\gamma}N\sqrt{\kappa^2+\rho^2}\ . \tag{3}$$

The latter is accumulated along the undulator, composed of N periods. The explicit expression for the UR resonance frequencies, containing the angles, reads as follows:

$$\omega_n = \frac{2n\omega_0\gamma^2}{1+(k^2\varpi/2)+(\gamma\theta)^2+(\gamma\theta_H)^2-(\gamma^2\theta_H\theta\sqrt{3}\,(\rho\sin\varphi-\kappa\cos\varphi)/\sqrt{\kappa^2+\rho^2})}\ . \tag{4}$$

In the absence of the constant field, which is largely screened out or compensated after careful evaluation of the field integrals, the UR line has common *sinc*-function shape and the UR differential intensity reads as follows:

$$\frac{d^2I}{d\omega d\Omega} = \frac{e^2N^2k^2}{\gamma^2c\left(1+\left(k_{eff}^2/2\right)+(\gamma\Theta)^2\right)}\sum_{n=-\infty}^{\infty}n^2\,\mathrm{sinc}^2\left(\frac{\nu_n}{2}\right)\left(f_{n;x}^2+f_{n;y}^2\right), \tag{5}$$

where $\nu_n = 2\pi nN\left(\left(\lambda_n/\lambda\right)-1\right)$ is the detuning parameter for the observed wavelength λ off the UR resonances λ_n, $f_{n;x,y}$ are the Bessel coefficients for x- and y-polarizations of the UR. The account for the electron energy spread σ_e can be done analytically by computing the following convolution: $\int_{-\infty}^{+\infty}d^2I\left(\nu_{\mathrm{n}}+2\pi nN\varepsilon\right)e^{-\varepsilon^2/2\sigma_e^2}\,d\varepsilon/d\omega d\Omega\sqrt{2\pi}\sigma_e$. The Bessel coefficients $f_{n;x,y}$ are specific for the undulator field. For example, upon computing the radiation integral for (1), we get with account for the off-axis angles the following Bessel coefficients:

$$f_{n;x} = \left|\left(J_{n+1}^n+J_{n-1}^n\right)+\frac{d}{h}\left(J_{n+m}^n+J_{n-m}^n\right)+\frac{2}{k}\gamma\theta\cos\varphi J_n^n\right|,\quad f_{n;y} = \left|\frac{2}{k}\gamma\theta\sin\varphi J_n^n\right|, \tag{6}$$

involving the following generalized Bessel function J_n^m:

$$J_n^m = \int_0^{2\pi}\frac{d\alpha}{2\pi}\cos\left[n\alpha+\frac{mk^2\left(\xi_0(\alpha)+\xi_1(\alpha)+\xi_2(\alpha)+\xi_3(\alpha)+\xi_4(\alpha)+\xi_5(\alpha)\right)}{1+\gamma^2\theta^2+\left(k_{eff}^2/2\right)}\right],$$

$$\xi_0 = \frac{2d\gamma\theta\cos\varphi\sin(h\alpha)}{kh^2},\ \xi_1 = \frac{\sin(2\alpha)}{4},\ \xi_2 = \frac{d\sin((h-1)\alpha)}{h(h-1)}, \tag{7}$$

$$\xi_3 = \frac{d\sin((h+1)\alpha)}{h(h+1)},\ \xi_4 = \frac{d^2\sin(2h\alpha)}{4h^3},\ \xi_5 = \frac{2}{k}\gamma\theta\cos\varphi\sin\alpha.$$

Formulae (6) are valid for any planar undulator; they account explicitly for the field harmonic dH_0 and for the angles θ и φ, differently from the formulae in [15]–[18],[40],[41], where the angular dependence was

incomplete. Note that (6) contains both explicit angular dependence of the Bessel coefficients $f_{n;x,y}$ (see $f_{n;y}$ and the last term in $f_{n;x}$) and the implicit dependence in J_n^m. This allows analytical study of the off-axis effects on the FEL radiation, done in what follows in section 4. The study of the UR from elliptic undulators can be done similarly, following the basic formulae for the Bessel coefficients in [16]. The effect of the undulator field harmonic in (1) was analyzed, for example, in [16], [17]; it was concluded, that for $k > 1.5$, $d > 0$ and $h = 3$ in (1) high UR harmonics become slightly more intense and the fundamental gets slightly weaker. This effect is felt mostly for $d \approx +0.5$ and it increases with the increase of the undulator parameter k. Higher field harmonics with h=5, 7, … have weak effect on the UR, which is in line with the conclusion in [46]–[48] that the radiation field is mainly formed by the 1st and 3rd undulator field harmonics.

For the following general configuration of the elliptic undulator field with the main period $\lambda_{u,x} \equiv \lambda$:

$$\begin{gathered}\vec{H} = H_0\left(\sin(k_\lambda z) + d\sin\left(pk_\lambda z\right), d_1\sin(hk_\lambda z) + d_2\cos(lk_\lambda z), 0\right), \\ k_\lambda = 2\pi/\lambda_{u,x},\ d, d_1, d_2 \in \text{reals},\ h, l, p \in \text{integers},\end{gathered} \tag{8}$$

we get the radiation wavelength (2) modified: $\varpi = 1 + \left(d/p\right)^2 + \left(d_1/h\right)^2 + \left(d_2/l\right)^2$. Calculating the radiation integral for the field (8), we get the following Bessel coefficients for the x- and y- polarizations:

$$\begin{aligned} f_{n;x} &= \left|\frac{d_1}{h}\left(J^n_{n+h} + J^n_{n-h}\right) + i\frac{d_2}{l}\left(J^n_{n+l} - J^n_{n-l}\right) + \frac{2}{k}\gamma\theta\cos\varphi J^n_n\right|, \\ f_{n;y} &= \left|\left(J^n_{n+1} + J^n_{n-1}\right) + \frac{d}{p}\left(J^n_{n+m} + J^n_{n-m}\right) + \frac{2}{k}\gamma\theta\sin\varphi J^n_n\right|, \end{aligned} \tag{9}$$

where the generalized Bessel functions have the following integral form:

$$J^m_n\left(\xi_i\right) = \int_{-\pi}^{\pi}\frac{d\alpha}{2\pi}\exp\left[i\begin{pmatrix} n\alpha + \xi_1\sin(h\alpha) + \xi_2\cos\left(l\alpha\right) + \xi_3\sin\alpha + \xi_4\sin\left(2\alpha\right) \\ +\xi_5\sin\left(2h\alpha\right) + \xi_6\sin(2l\alpha) + \xi_7\cos((l+h)\alpha) + \xi_8\cos((l-h)\alpha) \\ +\xi_0\sin(p\alpha) + \xi_9\sin((p+1)\alpha) + \xi_{10}\sin((p-1)\alpha) + \xi_{11}\sin\left(2p\alpha\right)\end{pmatrix}\right], \tag{10}$$

and they depend on the following arguments:

$$\xi_0 = \frac{8d}{kp^2}\gamma\theta\sin\varphi\xi_4,\ \xi_1 = \frac{8d_1}{kh^2}\gamma\theta\cos\varphi\xi_4,\ \xi_2 = \frac{8d_2}{kl^2}\gamma\theta\cos\varphi\xi_4,\ \xi_3 = \frac{8}{k}\gamma\theta\sin\varphi\xi_4, \tag{11}$$

$$\xi_4 = \frac{1}{4}\frac{mk^2}{1 + \left(\varpi k^2/2\right) + \gamma^2\theta^2},\ \xi_5 = \frac{d_1^2}{h^3}\xi_4,\ \xi_6 = -\frac{d_2^2}{l^3}\xi_4,\ \xi_7 = \frac{4d_1d_2}{hl(l+h)}\xi_4, \tag{12}$$

$$\xi_8 = \frac{4d_1d_2}{hl(l-h)}\xi_4,\ \xi_9 = \frac{4d}{p(p+1)}\xi_4,\ \xi_{10} = \frac{4d}{p(p-1)}\xi_4,\ \xi_{11} = \frac{d^2}{p^3}\xi_4. \tag{13}$$

The constant magnetic field in the undulator causes undesirable deviation of the electrons off the axis. This disrupts the transversal electron oscillations along the undulator axis and distorts the shape of the UR spectral line: instead of the common *sinc* function in (5), the generalized Airy-type function $S\left(\nu_n, \eta, \beta\right)$ arises [43]:

$$S\left(\nu_n, \eta, \beta\right) \equiv \int_0^1 \exp\left[i\left(\nu_n\tau + \eta\tau^2 + \beta\tau^3\right)\right]d\tau, \tag{14}$$

depending on the detuning parameter ν_n and containing the angular dependence:

$$\eta = \frac{4\pi^2N^2nk\gamma\theta}{1 + \left(k_{eff}^2/2\right)}\left(\kappa\cos\varphi - \rho\sin\varphi\right),\ \ \beta = \left(2\pi nN + \nu_n\right)\frac{\left(\gamma\theta_H\right)^2}{1 + \left(k_{eff}^2/2\right)} \cong 2\pi nN\frac{\left(\gamma\theta_H\right)^2}{1 + \left(k_{eff}^2/2\right)}. \tag{15}$$

In the constant magnetic field even UR harmonics appear on the axis with the polarization parallel to the periodic undulator field, just as they appear due to the betatron oscillations; the expression (5) for the UR intensity then changes to the following:

$$\frac{d^2I}{d\omega d\Omega} \cong \frac{e^2N^2\gamma^2k^2}{c(1+k^2/2)^2}\sum_{n=-\infty}^{\infty} n^2\left\{S^2\left(\nu_n,\eta,\beta\right)\left(f_{n;x}^2+f_{n;y}^2\right)+\left(\sqrt{3}\partial S/\partial\nu_{\rm n}\right)^2\left(f_{n,y}^H\right)^2\right\}, \tag{16}$$

where the following expression describes the induced by the field H_d Bessel coefficient $f_{n,y}^H$:

$$f_{n,y}^H = 2\gamma\theta_H J_n^n/k, \tag{17}$$

which resembles the last terms, $f_{n;x,y}^2 \sim 2\gamma\theta J_n^n/k$, in the common Bessel coefficients (6), (9) due to the off the axis angle θ. For the vanishing constant magnetic components $H_x=\rho H_0$, $H_y=\kappa H_0$, the $S(x,y,z)$ function reduces to the well-known *sinc* function: $S\left(\nu_n,0,0\right)=e^{i\nu_n/2}\,\mathrm{sinc}\left(\nu_n/2\right)$. The details of the relationship of the generalized Airy function $S(x,y,z)$ and its derivative with the generalized forms of Hermit polynomials and the exponential differential operators were discussed in [49]. We demonstrate graphically the behaviours of $S(\nu_n,\pm\pi,\beta)$ in Fig. 1 and of its derivative $\partial S(\nu_n,\pm\pi,\beta)/\partial\nu_n$ in Fig. 2.

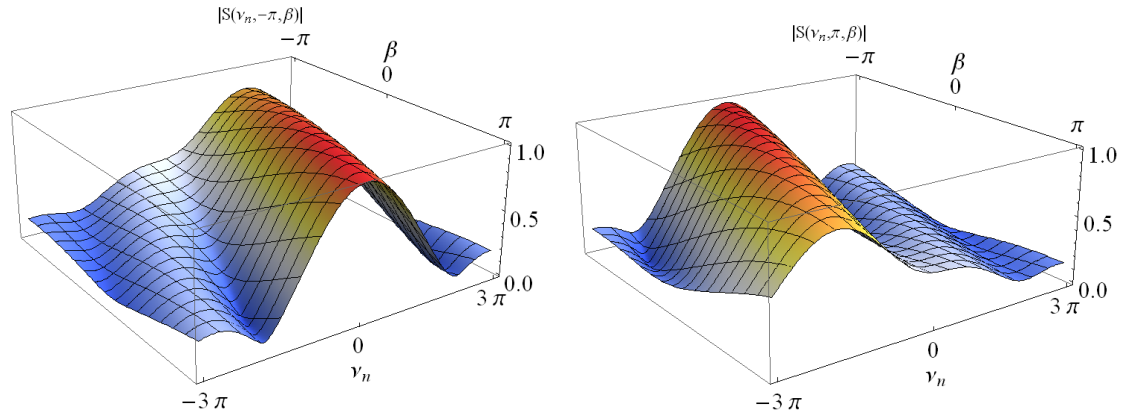

Fig. 1. Absolute values of the Airy-type function S for ν_n and β; $\eta=-\pi$ (left plot) and $\eta=+\pi$ (right plot).

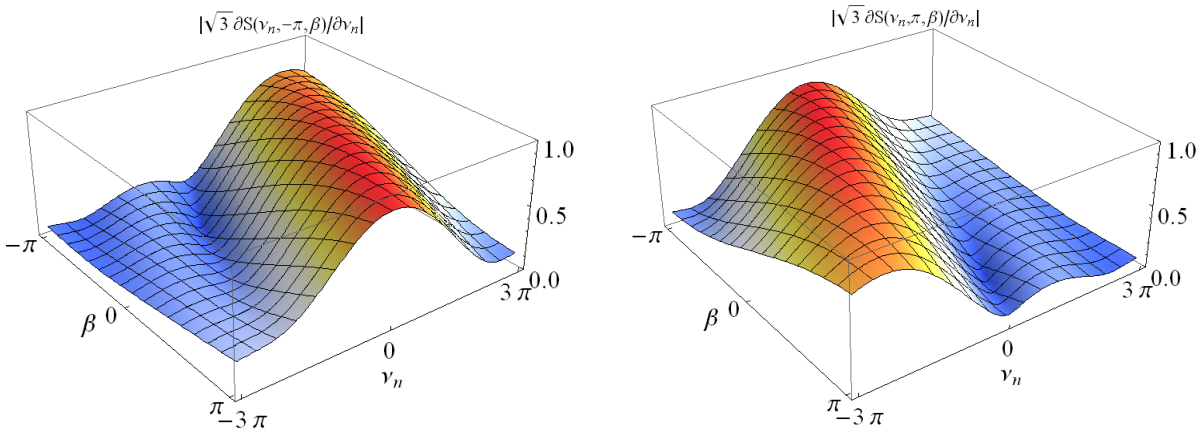

Fig. 2. Absolute values of the derivative $\sqrt{3}\partial S/\partial\nu_{\rm n}$ for ν_n and β; $\eta=-\pi$ (left plot) and $\eta=+\pi$ (right plot).

The induced angle θ_H is accounted for in β (15), and the off-axis angle θ is accounted for in η; the maximums are: $\max S=1$ and $\max\partial S/\partial\nu_{\rm n}=0.5$. The function $\partial S/\partial\nu_{\rm n}$ describes the shape of the even harmonics due to the constant magnetic field components in (1) with *y*-polarization, parallel to the periodic undulator field. The spectral line has its maximum at the nonzero value of the detuning parameter $\nu_n\approx-(\beta+\eta)$, $\nu_n,\beta,\eta\in[-2\pi,2\pi]$. This is different from the common case, $\eta=\beta=0$, in which the peak of the spectral line is at $\nu_n=0$. Note also that the induced bending angle θ_H can in part compensate the effect of the divergence angle θ on the UR spectrum. Indeed, it follows from the condition of the

maximum, $\nu_n \approx -(\beta+\eta)$, that the radiation in the angle $\bar{\theta} = \frac{k}{\gamma}\frac{2\pi N(\kappa^2+\rho^2)}{3(\rho\sin\varphi-\kappa\cos\varphi)}$ in the presence of the constant magnetic components ρ, κ, has the usual UR spectrum, $\omega_n = 2n\omega_0\gamma^2/1+(k^2\varpi/2)$, and its peaks at ν_n=0. For ρ=0 or κ=0 the expressions simplify without the sacrifice of physical generality: for example, for ρ=0 we get the angle $\widetilde{\theta} \approx \frac{2\pi}{3}\frac{k}{\gamma}N\kappa \approx \sqrt{3}\theta_H$, in which ν_n=0. The constant field induced Bessel coefficient (17) depends on the angle θ_H, induced by the field $H[T] = \frac{\sqrt{3}\gamma\theta_H}{2\pi\lambda_u[cm]N}$; the role of θ_H is similar to that of the deviation angle θ in $f^2_{n;x,y}$. Our calculations demonstrate that for the perceivable effect there should be the angle $\gamma\theta_H \approx 0.1$ accumulated along the undulator; such angle in a long undulator can be caused by a weak constant field constituent. For example, in the LEUTL FEL [23] it can be caused by the magnetic field $H = 1.2$ Gauss, in LCLS FEL [20], [22] $H = 0.8$ Gauss is enough, and in POHANG PAL-XFEL [36] the field $H = 0.5$ Gauss can induce this bending angle in a single undulator section. Thus, in long undulators for even the Earth field can cause significant off-axis deviation, if it is not screened out. If such magnetic components originate from defects of the magnetization in undulator magnets they are carefully evaluated and compensated.

Another well known effect is due to that ideal sinusoidal magnetic field $H_y = H_0\sin(k_\lambda z)$ does not satisfy Maxwell equations in the whole beam section. Thus, the additional magnetic components must be accounted for in both polarizations; for the common planar undulator [50]–[54] they read $H_y = H_0\sin(k_\lambda z)\cosh(k_\lambda y)$ and $H_z = H_0\cos(k_\lambda z)\sinh(k_\lambda y)$. For the bi-harmonic undulator (1) the concept remains the same [58] and the betatron oscillations with the frequency

$$\omega_\beta = \sqrt{2}\pi ck\delta/\lambda_n n\gamma = 2\sqrt{2}\pi c\gamma k\delta/\lambda_u\left(1+\left(k^2/2\right)\right), \quad \delta = \sqrt{1+d^2}\,, \tag{18}$$

appear (see [58] for the details), where d is the field harmonic parameter in (1), δ=1 in the common planar undulator for d=0. This results in the fine split of every UR harmonic in several betatron subharmonics, separated from each other by the inverse of the relativistic factor γ (18). This effect was discovered in the middle of the 20th century, when the electron beams had relatively low energies. For X-ray FELs, where $\gamma\sim10^3\div10^4$ we have $\omega_\beta \propto \omega_n/\gamma << \omega_n$ and the relative split of the spectral line is very fine. The betatron subharmonics are very close to each other and the interaction with the optical field occurs for all reasonable close subharmonics p of the harmonic n; the values vary: p=±2 ÷ ±7 (see examples in section 4). In the common undulator (see [50]–[54]) and in the bi-harmonic undulator (1) (see [58]) the betatron oscillations give rise to the additional Bessel functions $\widetilde{J}_p$:

$$\widetilde{J}_p(\xi,\zeta) = \int_0^{2\pi}\cos(pq-\zeta\sin q-\xi\sin 2q)dq/2\pi\,, \tag{19}$$

which factorize the Bessel coefficients (6), (9) of the split line: $f_{n;x,y} \to \sum_p \widetilde{J}_p(\xi,\zeta)f_{n;x,y}$ [50]–[58]. The above described effect depends on the initial position y_0 of the electron in the beam and on the deviation of its trajectory off the axis in the angle θ through the following dependence of the arguments:

$$\xi = \frac{\pi^2 y_0^2 k\delta}{2n\gamma\sqrt{2}\lambda_u\lambda_n} = \frac{\pi^2\gamma y_0^2 k\delta}{\sqrt{2}\lambda_u^2\left(1+\left(k^2/2\right)\right)}, \quad \zeta = \frac{2\pi\theta y_0}{n\lambda_n} = \frac{4\pi\theta y_0\gamma^2}{\lambda_u\left(1+\left(k^2/2\right)\right)}, \tag{20}$$

In practical terms, even if the spectral line in X-ray FEL is split due to the finite beam size and many betatron subharmonics are radiated with their respective numbers p, the effective frequency split is minor: $\omega_\beta \le 10^3\omega_n$; the total contribution of the first relevant subharmonics is usually enough close to unity. The examples for certain FELs will be given in the following section.

Off the axis position of the electron in the finite sized beam also gives rise to the weak even harmonics of the UR, whose polarization is in the plane of the undulator magnetic field. This polarization is orthogonal to that of the main radiation from the undulator, just like that of the even harmonics due to the

constant magnetic field, characterized by the Bessel coefficients (17). As compared with the contributions to the even harmonics, described by the last terms in the Bessel coefficients (6) and (9), which have both *x*- and *y*- polarizations and arise for off–axis angles $\theta \neq 0$, the even harmonics due to the betatron split are present on the undulator axis for $\theta=0$. The even betatron harmonics in the considered fields (1) or (8) are analytically accounted for by the following Bessel coefficients in complete agreement with [50]–[58]:

$$f^{\beta}_{n,p;y} \cong \left(\widetilde{J}_{p+1}(\xi,\zeta) - \widetilde{J}_{p-1}(\xi,\zeta)\right) J^{n}_{n} \sqrt{2}\pi y_0 \delta / \lambda_u \,, \tag{21}$$

where J^{n}_{n} are the proper Bessel functions, (7) or (10), dependently on the field (1) or (8), *n* is the harmonic number, $\widetilde{J}_{p}$ are the betatron Bessel functions (19), *p* is the betatron subharmonic number. Betatron oscillations effect the UR practically the same way for the undulator with or without field harmonic *d* in (1) and $d_{1,2,3,}$ in (8). In the common planar undulator $d=0$, $\delta = \sqrt{1+d^2}\Big|_{d=0} = 1$ and simpler functions $\widetilde{J}_n(\widetilde{\xi},\widetilde{\zeta})$ (19), where $\widetilde{\xi} = -nk^2/\left(4\left(1+\left(k^2/2\right)\right)\right)$, $\widetilde{\zeta} = 8\widetilde{\xi}\gamma\theta/k$, appear in (21) instead of the Bessel functions J^{n}_{n} (see (7) or (10)) for the multi-harmonic undulator fields. Evaluations show that in the case of relativistic beams with the factor $\gamma \sim 10^3 \div 10^4$ the even betatron Bessel coefficients $f^{\beta}_{n,p;y}$ (21) are very small, and their contribution, $f^{\beta}_{n,p=0;y} \sim 10^{-2}$, is minor as compared with that of the Bessel coefficients (6) or (9): $f_{n=1,3,5} \sim 0.8, 0.3, 0.15$. Our estimations for real beams also show that the even harmonics contributions due to the angles θ in (6) or (9) and θ_H in (16) usually exceed the contribution (21) due to the betatron oscillations. The examples for certain FELs are considered in the following section.

Before we proceed with the analysis of the harmonic generation in some FELs, we would like to underline that the above analytical approach is universal and it can be applied to practically any undulator. The results are obtained in the analytical form and this allows separate individual analysis of the contribution from different factors, such as the divergence, off the axis position, energy spread etc.

3. The analytical description of the harmonic power evolution in single-pass FELs

The above developed analytical approach can be applied to the stimulated radiation in free electron lasers, but it requires the analytical model of the FEL. The exact analytical solution to the complex set of the equations of motion and interaction of charges and radiation in the beam is not available. The solution to a 3rd order differential equation by the logistic function was proposed in [55]; it gave approximation for the power and bunching evolution along FELs. The application for the FEL harmonics behaviors was done in [25], [56]. The basic behaviors of the harmonic powers were described by the linear and nonlinear exponential terms, developing the FEL theory in [27], [28] et al; the first comparisons with the numerical simulations were performed and the results were promising; the relevant formulae were summarized in [57]. Since then the model has turned from a theoretical exercise to rather accurate analytical tool, which allows studying the FEL the spectrum characteristics, the harmonics behaviors and the underlying reasons for them and on any PC or even an engineering calculator by any user, not specialized in computer programming. The Bessel coefficients f_n for the spontaneous UR, obtained in the previous section, are involved in the phenomenological equations for the stimulated single-pass FEL harmonic powers with account for the major loss factors, considered separately for each harmonic *n* with account for their different sensitivity to the losses. Below we briefly present the model equations and explain their roles.

The key to the modeling is the Pierce parameter ρ_n [8], [9], which determines the amplification in a single pass FEL. With account for the diffraction it becomes $\widetilde{\rho}_n$ (see [57]):

$$\rho_{\mathrm{n}} = \frac{J^{1/3}\left(\lambda_u k_{eff} f_n\right)^{2/3}}{2\gamma\left(4\pi i\right)^{1/3}}\,,\ \widetilde{\rho}_n = \frac{\rho_n}{\left(1+\mu_{D,n}\right)^{1/3}},\ \mu_{D,n} = \frac{\lambda_u \lambda_n}{16\pi\rho_n \Sigma}\,, \tag{22}$$

where *n* is the harmonic number, f_n is the *n*-th harmonic Bessel coefficient, $\Sigma = 2\pi\sqrt{\beta_x \varepsilon_x \beta_y \varepsilon_y}$ is the electron beam cross section, related to the emittances $\varepsilon_{x,y} = \sigma_{x,y}\theta_{x,y}$, transversal sizes $\sigma_{x,y} = \sqrt{\varepsilon_{x,y}\beta_{x,y}}$ and divergences $\theta_{x,y}$, $\beta_{x,y} = \varepsilon_{x,y}/\theta^2_{x,y}$ and $\gamma_{x,y}$ are the Twiss parameters; $J = I_0/\Sigma$ [A/m^2] is the cur-

rent density, I_0 [A] is the beam current, $i \cong 1.7045 \times 10^4$ [A] is the Alfven current constant, λ_u is the main undulator period [m], λ_n is the n-th harmonic wavelength (see (2)), $k_{eff} = k\sqrt{\varpi}$ is the undulator parameter in a multiharmonic undulator, which reduces to $k = H_0 \lambda_u e / 2\pi mc^2 \approx H_0 \lambda_u [\mathrm{T\,cm}]$ in a common planar undulator, H_0 is the amplitude of the magnetic field on the undulator axis, e is the electron charge, m is the electron mass, c is the speed of light. The Pierce parameter ρ determines the FEL gain; for the n–th harmonic it reads $L_{n,g} \cong \Phi_n \lambda_u / 4\pi\sqrt{3} n^{1/3} \widetilde{\rho}_n$, $L_{1,g} \equiv L_g$, where the losses are accounted by the correction factor Φ_n defined in what follows.

Our current description of the FEL harmonic power evolution differs noticeably from that in early works [25], [55]–[57], where the losses for each FEL harmonic were accounted in the same way, and the saturation was described as a simple step from the exponential growth to a constant power level. Upon comparison with FEL experiments and numerical simulations, we have admitted that the early semi-analytical model gave just qualitative agreement. The actual understanding of the FEL processes [3]–[9], [22]–[24], [28], [29], [30]–[32] et al, and the numerical simulations, performed in [15], [40], [41], [59] to calibrate the phenomenological model, as well as the comparison with FEL experiments yield the conclusion that the saturation can be correctly described by the two stages, and the oscillations of the saturated power must be introduced. The attempt to remediate the problem by a single non-linear term in the model resulted in too low saturated power in [40], [59], which described the initial stage of the saturation process, or in too early saturation, where full power was reached in one-step from the nonlinear growth [41]. Thus, while the independent harmonic power growth $\propto e^{z/L_{n,g}}$ and basic nonlinear harmonic generation terms $\propto e^{nz/L_g}$ were verified in [25], [55], [56], the further nonlinear power growth close to saturation was not reproduced correctly for SACLA, LCLS, LEUTL and other FELs. For the realistic description of the harmonic behaviors in real devices, we introduce for the radiated power of the n-th FEL harmonic besides the linear on the logarithmic scale term also two non-linear terms $Q_{1,2n}$:

$$P_n(z) = P_{Ln}(z) + Q_{1n}(z) + Q_{2n}(z) + N_n(z), \tag{23}$$

where the linear on the logarithmic scale term P_{Ln} describes the independent growth of the n-th harmonic power in the unbunched beam from the initial power $P_{n,0}$ to the final power $P_{n,F}$ [56], [57]:

$$P_{Ln}(z) \cong \frac{P_{0,n} A(n,z) e^{0.223 z/L_s}}{1 + \dfrac{1.3 P_{0,n}\left(A(n,z) - 1\right)}{P_{n,F}\left(1 + 0.3\cos\left(\dfrac{n(z - L_s)}{1.38 L_g}\right)\right)}}, \quad A(n,z) \cong \frac{1}{3} + \frac{\cosh\dfrac{z}{L_{n,g}}}{4.5} + \frac{\cos\dfrac{\sqrt{3}z}{2L_{n,g}} \cosh\dfrac{z}{2L_{n,g}}}{0.444}. \tag{24}$$

The following undulator cascade gets the prebunched beam, where the independent power growth proceeds $\propto e^{z/L_{n,g}}$ until saturation, and if the latter is reached, then the saturated power oscillates with the period close to the FEL gain L_g due to the periodic energy transfer from the electrons to the photons and back as follows:

$$P_{L,n}(z) \cong \frac{P_{0,n} S_n(z)}{1 + 1.3 P_{0,n} S_n(z) / P_{n,f}\left(1 + 0.3\cos\left(n(z - L_s)/1.3 L_g\right)\right)}, \tag{25}$$

where S_n is the route of the partial differential equation of the 3rd order [56]:

$$S_n(z) \cong 2\left|\cosh\frac{z}{L_{n,g}} - e^{-\frac{z}{2L_{n,g}}}\cos\left(\frac{\pi}{3} + \frac{\sqrt{3}z}{2L_{n,g}}\right) - e^{-\frac{z}{2L_{n,g}}}\cos\left(\frac{\pi}{3} - \frac{\sqrt{3}z}{2L_{n,g}}\right)\right|, \tag{26}$$

Our numerical simulations in [15], [40], [41], [59] as well as the simulations in other works show that the oscillation period is ≈1.3–1.4L_g. Moreover, following these simulations and the FEL experimental data, we introduce two nonlinear terms $Q_{1,2n}$ for the induced harmonic power instead of the single term as discusses above. In the particular case, when the by fundamental tone is suppressed and another harmonic

dominates, the fundamental power must be substituted by that of the dominant harmonic, which saturates beyond the fundamental and generates subharmonics [16]. Omitting this special case, which is not considered in the present paper, we write two induced nonlinear power terms as follows:

$$Q_{1,n}(z) \cong \frac{\tilde{P}_{n,0} e^{n z/L_g}}{1+\left(\exp\left(n z/L_g\right)-1\right)\dfrac{\tilde{P}_{n,0}}{\tilde{P}_{n,F}}},$$
$$Q_{1,n}(z) \cong \frac{P_{n,0} e^{n z/L_g}}{1+\dfrac{\left(e^{n z/L_g}-1\right)1.3P_{n,0}}{P_{n,F}\left(1+0.3\cos\left(n\left(z-L_s\right)/1.3L_g\right)\right)-0.3\tilde{P}_{n,F}}}, \tag{27}$$

where $Q_{1,n}$ describes the preliminary saturation stage at the power level $\tilde{P}_{n,F}$ and $Q_{2,n}$ describes final saturation stage with the proper saturated oscillations around the power $P_{n,F}$. One more distinguishing difference of the present description consists in that the nonlinear contribution accounts for more sensitive electron-wave interaction at high harmonic wavelengths and updates all preceding versions of the model in [15]–[17], [33]–[35], [40], [41], [60] etc. The last term in (23) is due to the initial shot noise in the bunch and it can be formulated phenomenologically based on the available data for LEUTL, SPARC and other FEL experiments and on our previous numerical simulations in [15], [40], [41], [59], as follows:

$$N_n(z) \cong \frac{P_{\text{noise}}}{9n}\frac{S_n(z)}{1+30P_{\text{noise}}S_n(z)/nP_{n,f}}. \tag{28}$$

In the above formulae the initial powers $P_{n,0} \cong nb_n^2 P_{n,F}$ and $\widetilde{P}_{n,0} \cong d_n b_n^2 \widetilde{P}_{n,F}$ for the nonlinear generation are induced by the bunching $b_n^2 \cong \left(P_{0,1}/9P_e\widetilde{\rho}_1\right)^n$, the saturated powers are $P_{n,F} = \eta_n P_F f_n^2/n^{5/2}f_1^2$, $\widetilde{P}_{n,F} = \widetilde{\eta}_n \widetilde{P}_F f_n^2/n^{5/2}f_1^2$, $\widetilde{P}_F = P_F\big|_{\eta_n\to\widetilde{\eta}_n}$, $d_n \cong \{1,3,8,40,120\}$. Other details and equations, regarding the FEL harmonic power and bunching in cascaded undulators, can be found in [57], [15]–[17], [25], [33]–[35], [40], [41] et al. However, some formulae in the above-cited earlier works are erroneous and outdated. The formulae of this paper overwrite those in the above works in the case of any contradiction. The account for the losses in real devices is done phenomenologically and individually for each harmonic *n* with the help of the following coefficients:

$$\Phi_n \cong \left(\zeta^n + 0.165\mu_{\varepsilon,n}^2\right)\exp\left(0.034\mu_{\varepsilon,n}^2\right),\ \widetilde{\Phi}_n = \Phi_n\big|_{\mu_{\varepsilon,n}\to\widetilde{\mu}_{\varepsilon,n}}, \tag{29}$$

$$\mu_{\varepsilon,n}(\sigma_\varepsilon, n) \cong 2\sigma_\varepsilon/\left(n^{1/3}\rho_n\right),\quad \widetilde{\mu}_{\varepsilon,n}(\sigma_\varepsilon, n) \cong 2n^{2/3}\sigma_\varepsilon/\widetilde{\rho}_n, \tag{30}$$

$$\eta_n \cong \left(e^{-\Phi_n(\Phi_n-0.9)} + 1.57\left(\Phi_n-0.9\right)/\Phi_n^3\right)/1.062,\quad \widetilde{\eta}_n = \eta_n\big|_{\Phi_n\to\widetilde{\Phi}_n}, \tag{31}$$

$$\zeta \cong \sqrt{\prod_{i=x,y,\widetilde{x},\widetilde{y}}\left(1+\mu_i^2\right)}\Bigg/\left(1+0.159\sum_{i=x,y,\widetilde{x},\widetilde{y}}\mu_i^2 - 0.066\sum_{i=x,y,\widetilde{x},\widetilde{y}}\mu_i\right), \tag{32}$$

$$\mu_{\widetilde{x},\widetilde{y}} = \frac{1}{\widetilde{\rho}_1}\frac{\gamma^2\varepsilon_{x,y}}{(1+k_{eff}^2)\lambda_u\beta_{x,y}},\ \mu_{x,y} = \frac{1}{\widetilde{\rho}_1}\frac{\gamma^2\pi^2k^2\varepsilon_{x,y}}{(1+k_{eff}^2)\gamma^2\lambda_u^2\gamma_{x,y}}, \tag{33}$$

where μ_i (33) [56] in (32) in the matched beams yield the value $\zeta \approx 1.00-1.05$, and for X-ray FELs $\zeta = 1-1.02$ and the relevant correction is minor. The above formulae account for the fact that in real installations the Pierce parameter is smaller than the ideal, $\widetilde{\rho}_n < \rho_n$, the gain length $L_{n,g}$ is longer than the ideal and the saturated power $P_{n,F} = \eta_n P_F f_n^2/n^{5/2}f_1^2$, where $P_F \cong \sqrt{2}P_e\,\eta_1\widetilde{\rho}_1^2/\rho_1$, P_e is the beam power, is lower than the ideal. The saturation occurs at the length $L_s \cong 1.07L_{1,g}\ln\left(9\eta_1 P_F/P_{1,0}\right)$.

We would like to underline that while there is some theoretical background for the above formulae, they are largely phenomenological; nevertheless, they give quite good reproduction of the power evolution in both linear and nonlinear regimes as well as in the sensitive and complicated saturated regime. The noise contribution at the beginning of the FEL is also fairly well reproduced as can be seen in the following section. However, even complex numerical simulations, which solve the systems of equations for the fields and charges and trace the bunch and photon pulse evolution in the undulators in 3D, give discrepancy in their predictions up to one order of magnitude for the harmonic powers. The difference between the genuine simulations and the measurements is evident, for example for the PAL-XFEL in [36] and for the LEUTL FEL in [23], [24]. Moreover, in [61] the authors performed numerical simulations with several codes for the SPARC experiment. The difference between the results of the simulations for the fundamental tone was more than 5 times at the end of the FEL and more than 10 times at the beginning of the FEL; for the 3rd FEL harmonic the difference between the simulation results was more that one order of magnitude at the saturation and more than two orders of magnitude at the beginning of the FEL. Thus, we should frame our results for the FEL experiments (see the following section) in this context. Our model has been verified with the FEL experiments in [15]–[17], [40]–[41], [60] and it gives good description of the power and bunching. The analytical model in its present formulation will be used in the following chapter for the analysis of the FEL harmonics.

4. Analysis of the harmonics radiation in some FEL experiments

The first FEL was operated at Stanford University in 1976. At present there are more than 50 light sources in the world see [62] (and links in it), [63], which are operational or under construction. There continue to be many experiments run at user facilities around the world. The operating FELs generate radiation in infrared, visible, ultraviolet (UV), and X-ray bands. Among them we have chosen some well known and recently documented examples to explore the harmonic generation in these installations. Our study is conducted analytically, with the help of rigorous formalism of the generalized Bessel functions (see section 2), coupled with the analytical phenomenological FEL model. In this study we have added the description of the oscillations of the saturated power in the phenomenological model. The key equations of the model are summarized in the Appendix.

LCLS FEL X-ray experiments

Let us consider the FEL experiment LCLS [20]–[22], where the soft and hard X-rays at the fundamental wavelengths λ_1=1.5 nm and λ_1=0.15 nm were obtained. The relevant data is collected and shown in Table 1 and in right plot in Fig. 3 for λ_1=1.5 nm "low energy" E=4.3 GeV experiment, and in Table 2 and in left plot in Fig. 3 for λ_1=0.15 nm "high energy" E=13.6 GeV experiment. The dots in the left plot denote the average measured values, the shadowed areas in both plots denote the expected values for the harmonic powers according to [20]–[22].

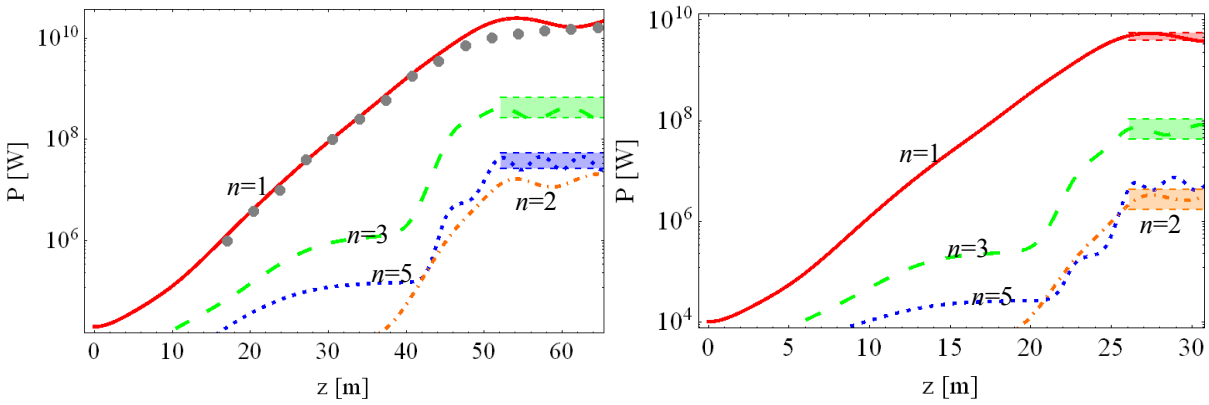

Fig. 3. The harmonic power evolution along the undulators in LCLS FEL experiments. Right plot — soft X-rays, λ_1=1.5 nm, and left plot — hard X-rays, λ_1=0.15 nm. The estimated in [22] harmonic power range is shown by the shadowed areas and the measured average values are shown by dots. The harmonics are color coded: n=1 — red solid line, n=2 — orange dot dashed line, n=3 — green dashed line, n=5 — blue dotted line.

Table 1. Some simulation data for LCLS FEL experiment for soft X-rays at λ=1.5 nm, *E*=4.3 GeV

Beam parameters: γ=8400, beam power P_E=4.29 TW, current I_0=1 kA, current density J=1.57×10^{11} A/m^2, beam section Σ =6.36×10^{-9} m^2, emittances $\gamma\varepsilon_{x,y}^{slice,135meV}=0.4$ μm, $\gamma\varepsilon_{x,y}^{projected,4.3GeV}\approx 0.85$ μm, β=10 m, beam size $\sigma_{x,y}$=30μm, divergence $\theta=$≈3μrad, energy spread σ_e=0.3×10^{-3}					
Undulator parameters: k=3.5, λ_u=3 cm, periods N=113, section length 3.4m					
FEL properties: saturated length L_s=26 m, gain length L_{gain}=1.6 m, radiation beam size $\sigma_{photon}\approx\sqrt{\sigma_{x,y}\sqrt{\lambda_1 L_g/4\pi}}$ ≈20 μm					
Harmonic number	n=1	n=2	n=3	n=4	n=5
Bessel coefficient f_n	0.74	0.09	0.33	0.10	0.20
Pierce parameter $\tilde{\rho}_n$	0.0009	0.0002	0.0006	0.0002	0.0004
Harmonic wavelength λ_n, nm	1.5	0.75	0.5	0.375	0.3
Saturated power $P_{F,n}$,W	5.3×10^9	4.2×10^6	6.6×10^7	2.4×10^6	7.2×10^6

All the modeled values reproduce well those measured experimentally and estimated by the LCLS team. The gain length L_{gain}=1.6 m, the saturation length L_s=26 m, the Pierce parameter ρ≈0.001, all fit well the data in [20]–[22]. There have been the 2nd and 3rd harmonics measured, and the 5th harmonic was estimated quantitatively. All the power values are in agreement with [20]–[22] (see Fig. 3), including the 2-nd harmonic power; the data for it only was available for the soft X-rays due to the tuning of the detectors for the frequency range, and filtering of the fundamental tone. It is interesting to find the reasons for the even harmonic generation in soft X-rays. In this experiment with γ=8400 and the current I=1kA [20]–[22] the electron beam size was $\sigma_{x,y}$≈30μm, the divergence θ≈3μrad, the optical beam had the size σ_γ≈20μm. The spectrum lines are split due to the betatron oscillations in the beam. The values of the subharmonic Bessel function (19) are $\left|\tilde{J}_{p\in[-3,+3]}\right|(\xi,\zeta)\cong\{0.05, 0.22, 0.57, 0.52, 0.55, 0.24, 0.07\}$. The Bessel coefficients (6) f_n are factorized by the above Bessel function $\tilde{J}_p(\xi,\zeta)$ (19). In the split of the harmonic line five subharmonics with p=0,±1,±2 give major contribution. The wavelength split between the subharmonics is minimal, δλ=λ/γ=0.00018nm, and the deviation from the resonance λ_1=1.5 nm for p=±2 gives the spectral line width Δλ~1pm where the subharmonics interfere with the optical pulse constructively. The relative line width is Δλ/λ≈5×10^{-4}. Thus due to highly relativistic beam, the radiation line split is hardly perceived even for the subharmonics p of the harmonic n, whose wavelength is λ_1/n. The contribution of the betatron term (21) with the y-polarization is very small: $f_{n,p;y}^{\beta}$~2×10^{-3} as compared with other contributions, such as that from the divergence angle, which gives $f_{2;y}$~2×10^{-2}. The term with the other x-polarization is larger, but not enough to explain the observed powers of the 2nd FEL harmonic. The real reason for the strong 2nd FEL harmonic must be the deviation of the electron trajectories off the axis by Δ~15μm on one gain length, reported in [20]–[22]; this deviation is within the photon beam size, but it forms the off-axis angle θ≈10 μrad. With account for that we obtain the harmonic powers, presented in the right plot in Fig. 3. Observe in Fig. 3 as the oscillating saturated powers of FEL harmonics are largely within the intervals, designated in [20]–[22]. The 3-rd harmonic has the power ~1.2% of the fundamental; the 2-nd harmonic rate is 0.08%, i.e. within the estimated range 0.04%–0.1%; the 5th harmonic is few percent of the 3rd. The level of the 3rd harmonic was generally measured at 1%–2.5%; occasionally it dropped to 0.2% [22]. Note that the magnetic field of the Earth, ~0.5 Gauss, would cause the beam deviation comparable with that reported and yield the result similar to that shown in Fig. 3.

Now let us consider the hard X-ray LCLS experiment [20]–[22] with γ=26600, E=13.6 GeV and the fundamental wavelength λ_1=0.15 nm. Some relevant data is collected in Table 2, the harmonic powers are shown in left plot in Fig. 3. The 1st harmonic power traces well the experimentally measured values at

each station; some disagreement is only in the oscillating peak part; this frequently occurs even for complicated 3D numerical simulations. Close to ideal agreement with the measurements is also for the simulated 3rd harmonic power, which is 1.3% of the fundamental in agreement with [22]. The 2nd harmonic was not measured; the 5th is correctly estimated at ~10% of the 3rd harmonic power. The agreement is good as seen in left plot in Fig. 3.

Table 2. Some simulation data for LCLS FEL experiment for hard X-rays at λ=0.15 nm

Beam parameters: γ=26600, beam power P_E=40.77 TW, current I_0=3 kA, current density J=6.09×10^{11} A/m^2, beam section Σ =4.926×10^{-9} m^2, emittances $\gamma\varepsilon_{x,y}^{slice,135meV}=0.4$ μm, $\gamma\varepsilon_{x,y}^{projected,13.6GeV}\approx 0.6$ μm, β=25.5 m, beam size $\sigma_{x,y}$=28μm, divergence θ≈0.9 μrad, energy spread σ_e=0.1×10^{-3}					
Undulator parameters: k=3.5, λ_u=3 cm, periods N=113, section length 3.4m					
FEL properties: saturated length L_s=52 m, gain length L_{gain}=3 m, radiation beam size $\sigma_{photon}\approx\sqrt{\sigma_{x,y}\sqrt{\lambda_1 L_g/4\pi}}$ ≈13 μm					
Harmonic number	n=1	n=2	n=3	n=4	n=5
Bessel coefficient f_n	0.74	0.06	0.33	0.07	0.22
Pierce parameter $\widetilde{\rho}_n$	0.0005	0.00009	0.0003	0.0001	0.0002
Harmonic wavelength λ_n, nm	0.15	0.075	0.05	0.0375	0.03
Saturated power $P_{F,n}$,W	2.2 ×10^{10}	1.9×10^7	3.5×10^7	7.0×10^6	4.0×10^7

The study of the spectrum line split shows that p=±4 first subharmonics contribute mostly; other are negligible. Proper Bessel coefficients (19) for p=0,±1,±2,±3,±4 read as follows: $\left|\widetilde{J}_{p\in[-4,+4]}\right|(\xi,\zeta)\cong\{0.1,0.28,0.50,0.40,0.23,0.34,0.47,0.31,0.13\}$. Despite the split is present more, than in the soft X-ray experiment, the subharmonics are separated by the step δλ/λ≈0.0000376, whose value is absolutely negligible even for the subharmonics with the number p=10 and more. Thus all of them participate in the FEL amplification process for the harmonic n. The even harmonic contribution from the betatron oscillations is expectably very small in X-ray FEL. We get comprehensively the values $f_{n,p;y}^{\beta}$~2×10^{-3} << $f_{2;y}$~2×10^{-2} , the latter is due to the off the axis angle. Due to some more narrow beams than in soft X-ray experiment, and much longer gain and smaller deviation of the beam, Δ~5μm [22] in the "high energy" case, the 2nd harmonic is weaker in hard X-ray LCLS experiment, than in soft X-ray LCLS experiment, despite the hard X-ray spectrum line in the split in more subharmonics. Thus, we get the total spectrum line width in hard X-ray Δλ≈0.05 pm for λ_1=0.15 nm wavelength, relative width is Δλ/λ≈3×10^{-5}. The beam deviation off the axis and the interaction of the radiation with the electrons on roughly one gain length mainly cause the radiation of even harmonics in this experiment. High harmonics are radiated also because of quite high undulator parameter value k=3.5. They are sensitive to the beam quality. Good quality beams with low energy spread ~10^{-4}, such as that in the LCLS experiment, allow their radiation.

LEUTL FEL experiments

In LEUTL FEL experiments [23], [24], differently from the X-ray LCLS experiments [20]–[22], the radiation close to visible wavelengths 530 nm and UV-A radiation at 385 nm were produced. We have subjected to theoretical analysis both cases, but for brevity we present here only the case of the radiation with the fundamental wavelength λ_1=530 nm. We refer to two latest series of experiments, where the 2nd and the 3rd harmonics were detected and measured along the undulators [23]. Some data for the modeling is collected in Table 3 and in Table 4 (the emittances are renormalized on γ; they were normalized on πγ in [23]); the results of the modeling are graphically presented in Fig. 4, where the comparison with the experimental values can be seen, following the data reported in [23]. The dots in the plot denote the aver-

age measured values; the shadowed areas denote the expected values for the harmonic powers, according to [23]. The authors of [23] noted high level of initial noise in their experiments on 30 March 2001, which affected the first undulator sections. This explains significant mismatch of the measured and analytically evaluated results at the beginning of the FEL (see left plot in Fig. 4 and the simulations in [23]). They significantly improved the setup in the succeeding experiment, added more stations for the 2nd harmonic measuring and reduced the disturbances. The right plot demonstrates very good agreement of our simulation with these clean experimental measurements, where the 2nd harmonic power evolution (orange dots and line) can be traced along the whole FEL.

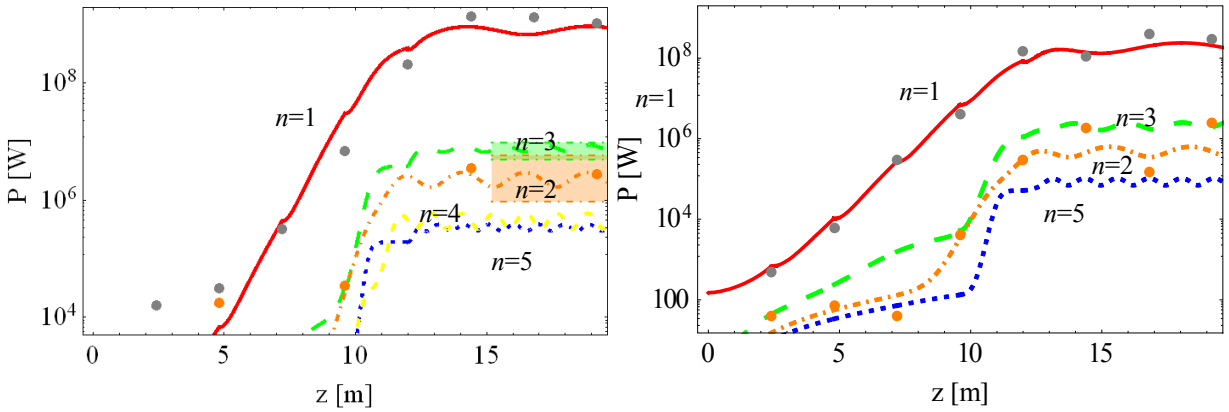

Fig. 4. The harmonic power evolution along the undulators in LEULT FEL experiment, λ_1=532 nm; left plot — simulation and data from 30 March 2001, right plot — from 16 August 2001. The estimated in [23] harmonic power range is shown by the shadowed areas; the measured values for the fundamental and the 2nd harmonics are shown by dots. The harmonics are color coded: *n*=1 — red solid line, *n*=2 — orange dot-dashed line, *n*=3 — green long-dashed line, *n*=4 — yellow medium-dashed line, *n*=5 — blue dotted line.

In the LEUTL FEL [23], [24], the electron beam had much bigger size than in the LCLS FEL [20]–[22], so one would expect noticeable 2nd FEL harmonic and the spectrum line split due the initial off-axis position of electrons in the beam, following (19), (21). Consider for certainty the latest LEUTL experiment and the data in Table 4. The beam with the emittances $\gamma\varepsilon_{x,y} = 2.0\,\mu$m and size $\sigma_{x,y}$=0.26 mm had the divergence $\theta \approx 18$ μrad. The electron current was I_0=210A, the electrons had the energy spread $\sigma_e=1\times10^{-3}$. This results the gain length L_{gain}=0.7 m and the saturation length L_s=12.5 m; the radiation beam size is $\sigma_{photon} \approx \sqrt{\sigma_{x,y}\sqrt{\lambda_1 L_g/4\pi}} \cong 0.21$ mm. Due to γ~500>>1 the first few subharmonic are close to each other and they all interact with the beam constructively. Moreover, the contribution of the betatron oscillations appears very small. In practical terms the Bessel coefficients for p=0,±1,±2 matter: $f^{\beta}_{n=2,p\in[-3,+3]} \cong \{0.001, 0.007, 0.008, 0.012, 0.007, 0.005, 0.002\}$, but their total contribution to the 2nd harmonic amounts to small value: $f^{\beta}_{n,p;y} \cong 2\times10^{-2}$. The contribution of the angular part in (6) of the same parallel polarization is comparably small: $f_{2;y} \cong 3\times10^{-2}$. Major contribution comes from the angular part in the usual orthogonal polarization in (6): $f_{2;x} \approx 10^{-1}$. Moreover, the harmonic split occurs mainly for p=0,±1,±2, which is evidenced by the values of proper Bessel function (see (19)): $\tilde{J}_{p\in[-5,+5]} = \{0.000, 0.002, 0.001, 0.098, 0.493, 0.721, 0.443, 0.171, 0.048, 0.011, 0.002\}$. The radiation line is split in 4–6 subharmonics, each distant by $\delta\lambda \cong \lambda/\gamma \cong 1.25$ nm; this yields the total spectral width $\Delta\lambda$~6nm, which is in perfect agreement with the spectral line width in plots in [23], where, for example, the 2nd harmonic was in the range $\Delta\lambda$~[266nm, 272nm]. This confirms that our calculations are correct and the conclusions are valid.

Table 3. Some simulation data for LEUTL FEL experiment at λ=532 nm, *E*=217 MeV from 03 March 2001

Beam parameters: γ=425, beam power P_E=109.6 GW, current I_0=505 A, current density J=8.41×10^8 A/m^2, beam section Σ =6.00×10^{-7} m^2, emittances $\gamma\varepsilon_{x,y} = 2.7$ μm, β=15 m, beam size $\sigma_{x,y}$=0.31 mm, divergence $\theta \approx$20 μrad, energy spread σ_e=1×10^{-3}					
Undulator parameters: k=3.1, λ_u=3.3 cm, periods N=75, section length 2.5 m					
FEL properties: saturated length L_s=11.7 m, gain length L_{gain}=0.55 m, radiation beam size $\sigma_{photon} \approx \sqrt{\sigma_{x,y}\sqrt{\lambda_1 L_g/4\pi}} \approx$0.22 mm					
Harmonic number	n=1	n=2	n=3	n=4	n=5
Bessel coefficient f_n	0.74	0.18	0.30	0.19	0.15
Pierce parameter $\tilde{\rho}_n$	0.0032	0.0012	0.0018	0.0013	0.0011
Harmonic wavelength λ_n, nm	531	266	177	133	106
Saturated power $P_{F,n}$,W	5.3×10^9	4.2×10^6	6.6×10^7	2.4×10^6	7.2×10^6

Table 4. Some simulation data for LEUTL FEL experiment at λ=532 nm, *E*=217 MeV from 16 August 2001

Beam parameters: γ=425, beam power P_E=45.57 GW, current I_0=210 A, current density J=4.79×10^8 A/m^2, beam section Σ =4.38×10^{-7} m^2, emittances $\gamma\varepsilon_{x,y} = 2.0$ μm, β=15 m, beam size $\sigma_{x,y}$=0.26 mm, divergence $\theta \approx$18 μrad, energy spread σ_e=1×10^{-3}					
Undulator parameters: k=3.1, λ_u=3.3 cm, periods N=75, section length 2.5 m					
FEL properties: saturated length L_s=12.5 m, gain length L_{gain}=0.7 m, radiation beam size $\sigma_{photon} \approx \sqrt{\sigma_{x,y}\sqrt{\lambda_1 L_g/4\pi}} \approx$0.21 mm					
Harmonic number	n=1	n=2	n=3	n=4	n=5
Bessel coefficient f_n	0.74	0.17	0.30	0.18	0.15
Pierce parameter $\tilde{\rho}_n$	0.0025	0.00094	0.0014	0.0011	0.00096
Harmonic wavelength λ_n, nm	531	266	177	133	106
Saturated power $P_{F,n}$,W	1.5×10^8	6.1×10^5	1.1×10^6	1.5×10^5	5.2×10^4

However, the computation of the Bessel factors with account for the beam size and emittances alone yields rather small values of the Bessel coefficients for the 2nd harmonic for *x*- and *y*-polarizations, $f_{2;x} \approx$0.045, $f_{2;y} \approx$0.002, unable to explain the observed 2nd harmonic power. The reason is different from that in the X-ray LCLS experiment. Indeed, in LEUTL experiment the radiation interacts on one gain length $L_{gain} \approx$0.7 m with the electrons in very wide section, $\sigma_{x,y} \approx$0.2 mm. This means that significant angles of the photon-electron interaction arise, $\bar{\theta} \approx \sigma_{x,y}/L_{gain} \approx$0.3 mrad, which exceed the divergence angle $\theta \approx$18 μrad by one order of magnitude. The respective normalized angle $\gamma\bar{\theta} \approx 0.13$ causes significant off-axis contributions and causes the split of the spectral line in 5–6 subharmonics as described above. The account for all these phenomena was performed analytically with the formalism presented in section 2 and in Appendix 6; the results appear in very good agreement with the experiments as seen in Fig. 4.

POHANG FEL X-ray experiments

In recent POHANG PAL-XFEL FEL experiments [36] the X-ray radiation with the wavelengths 1.52 nm and 0.144 nm was generated. We have addressed the harmonic generation in both soft and hard X-ray experiments; the comparison can be done with the data on the radiation of the fundamental tone, reported in [36]. Some modeling data is collected Table 5 and Table 6. The results are presented in Fig. 5 – Fig. 8 and discussed below.

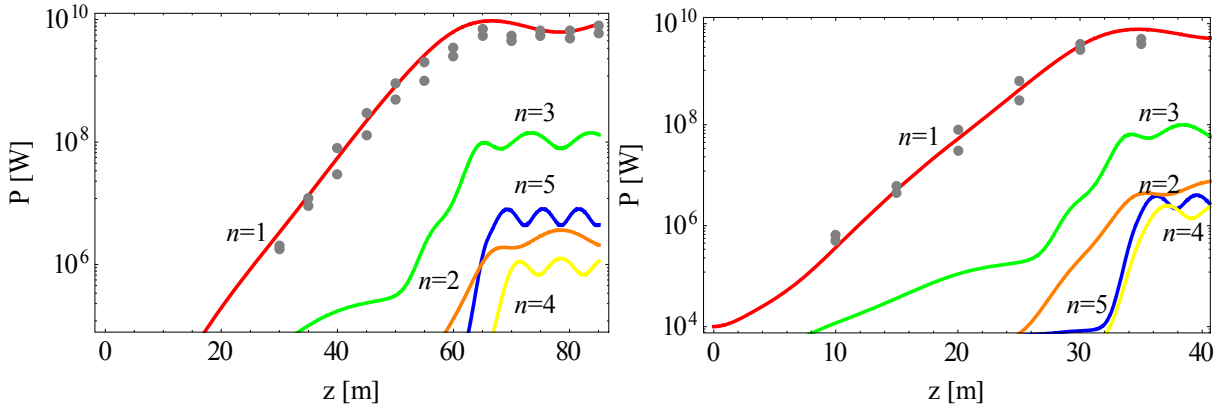

Fig. 5. The harmonic power evolution along the undulators in POHANG FEL experiments: right plot — soft X-rays, λ_1=1.52 nm, and left plot — hard X-rays, λ_1=0.144 nm. The experimental average values are shown by dots, following the data in [36]. The harmonics are color coded: *n*=1 — red line, *n*=2 — orange line, *n*=3 — green line, *n*=4 — yellow line, *n*=5 — blue line.

Table 5. Some simulation data for POHANG FEL experiment for soft X-rays, λ=1.52 nm, *E*=3 GeV

Beam parameters: γ=5870, beam power P_E=6.60 TW, current I_0=2.2 kA, current density J=1.246×10^{11} A/m^2, beam section Σ =1.766×10^{-8} m^2, emittances $\gamma\varepsilon_{x,y}$ = 0.55 μm, β=30 m, beam size $\sigma_{x,y}$=53 μm, divergence θ ≈1.8 μrad, energy spread σ_e=0.5×10^{-3}					
Undulator parameters: k=2, λ_u=3.5 cm, section length 5 m					
FEL properties: saturated length L_s=33 m, gain length L_{gain}=2.0 m, radiation beam size $\sigma_{photon} \approx \sqrt{\sigma_{x,y}\sqrt{\lambda_1 L_g/4\pi}}$ ≈0.29 mm					
Harmonic number	*n*=1	*n*=2	*n*=3	*n*=4	*n*=5
Bessel coefficient f_n	0.81	0.02	0.32	0.02	0.19
Pierce parameter $\tilde{\rho}_n$	0.0010	0.00007	0.0006	0.00008	0.0004
Harmonic wavelength λ_n, nm	1.52	0.76	0.51	0.38	0.30
Saturated power $P_{F,n}$,W	8.0×10^9	7.0×10^6	8.0×10^7	2.0×10^6	3.5×10^6

In PAL-XFEL POHANG experiments the radiation data is similar to that of LCLS experiments. The main difference is in the energy spread, which was higher in PAL-XFEL experiments, and the undulator parameter k, which was lower in the PAL-XFEL experiments. The soft X-ray radiation at λ_1=1.52 nm was produced by the electrons with the energy E=3GeV and the energy spread $\sigma_e^{soft} = 0.05\%$ (~5 times higher than in LCLS), in the undulators with the total pure length ~40 m; the undulator parameter was k=2. Hard X-ray radiation at λ_1=0.144 nm was generated by the electrons with the energy E=8 GeV (lower than E~13GeV in LCLS) with the spread $\sigma_e^{hard} = 0.018\%$ (~2 times higher than in LCLS) in the undulators with the parameter k=1.87 (vs. k=3.5 in LCLS) of the total pure length 100m. Each undulator section was 5 m long. Using the data from the experimental setup [36], we analytically obtained the curves of the FEL power evolution for the FEL harmonics as shown in right and left plots in Fig. 5 for the

soft and hard X-rays respectively with account for the beam size, divergences and effective angles of the photon–electron interaction in the beam. The results are compared with the measurements of the fundamental tone power. In Fig. 5 note as the match of our analytical simulations with the experiment is good; for soft X-rays in the exponential growth the agreement is better than that of the simulations in [36]. Our analytical results for the hard X-ray power evolution also agree with the measured values very well; the saturated power oscillations are reproduces some better than with the 3D numerical simulations in [36]. This evidences the correct analytical account for all underlying physical phenomena.

Table 6. Some simulation data for POHANG FEL experiment for hard X-rays, λ=0.144 nm, *E*=8 GeV

Beam parameters: γ=15660, beam power P_E=20.0 TW, current I_0=2,5 kA, current density J=2.83×10^{11} A/m^2, beam section Σ =8.825×10^{-9} m^2, emittances $\gamma\varepsilon_{x,y} \approx 0.55$ μm, β=40 m, beam size $\sigma_{x,y}$=37μm, divergence $\theta \approx$0.94 μrad, energy spread σ_e=0.18×10^{-3}					
Undulator parameters: k=1.87, λ_u=2.571 cm, section length 5 m					
FEL properties: saturated length L_s=60 m, gain length L_{gain}=3.4 m, radiation beam size $\sigma_{photon} \approx \sqrt{\sigma_{x,y}\sqrt{\lambda_1 L_g/4\pi}} \approx$15 μm					
Harmonic number	n=1	n=2	n=3	n=4	n=5
Bessel coefficient f_n	0.82	0.05	0.32	0.05	0.18
Pierce parameter $\tilde{\rho}_n$	0.0004	0.00006	0.0002	0.00006	0.00015
Harmonic wavelength λ_n, nm	0.144	0.072	0.048	0.036	0.029
Saturated power $P_{F,n}$,W	9.0 ×10^9	2.0×10^6	1.0×10^8	1.0×10^6	6.0×10^6

With regard to high harmonic generation there is no data available for this experiment. The energy spread was quite high as compared with the LCLS experiment, where the radiation wavelengths were similar. For soft X-ray PAL-XFEL $\sigma_e^{soft} = 0.0005 \cong \rho_1/2 \cong \rho_3 \cong 0.0006 > \rho_5 \cong 0.0004$. In terms of the emittance we get the pure value $\varepsilon \cong 0.94\times10^{-10}$ m to be compared with $\lambda_1/4\pi=1.2\times10^{-10}$ m. However, for the 5th harmonic we get $\lambda_5/4\pi=2.5\times10^{-11}$ m and $\varepsilon \cong \lambda_5/\pi=1\times10^{-10}$ m. The 3rd harmonic could appear with the power rate ~0.7% of the fundamental, the 2nd harmonic would have the power rate ~0.05%, as shown in Fig. 5. Our estimation for the 3rd harmonic at POHANG in soft X-rays, P_3/P_1 ~0.7%, amounts to the half of that at LCLS, P_3/P_1 ~1.3% for λ_3=0.5 nm [22] with similar radiation and parameters. So we can expect weaker 3rd harmonic at POHANG due to smaller value of the undulator parameter k as compared with LCLS; moreover, the detrimental effect of the energy spread is higher for PAL-XFEL, $\sigma_e = 0.0002 \div 0.0005$, as compared with that in LCLS, where $\sigma_e = 0.0001$. Pierce parameter for the 2nd harmonic at POHANG is very small, so it is unsurprising that high harmonics were not registered.

For hard X-rays the energy spread and Pierce parameters read as follows: $\sigma_e^{hard} = 0.00018 \cong \rho_1/2 < \rho_3 = 0.00021 > \rho_5 = 0.00015$, $\rho_2 = 0.00006$; these relations between σ_e and ρ_n are close to those for soft X-ray radiation. Moreover, for hard X-rays the comparison of the emittance $\varepsilon \cong 3.5\times10^{-11}$ m with $\lambda_3/4\pi=3.8\times10^{-12}$ m is not favorable and for the 3rd harmonic radiation: we get $\varepsilon_{x,y} \cong 10\times\lambda_3/(4\pi)$. Unsurprisingly, high harmonics were not detected in hard X-rays. However, if the energy spread and emittances are improved, then we could expect at the POHANG FEL the harmonic generation as suggested in Fig. 5. The beam deviations off the axis amounted to maximum ~10 μm on one undulator length. This causes the off-axis angle ~2μrad, comparable with the divergence, ~2μrad for soft X-rays and ~1μrad for hard X-rays. For the soft X-ray experiment the electron-photon interaction must be considered with the angle $\bar{\theta} \cong 14$ μrad, much exceeding the beam deviation. For hard X-rays, however, we get $\bar{\theta} \cong 4$ μrad and the beam must be kept on the axis more precisely. Possible effect of this angle on high harmonic generation (provided the harmonics are allowed by the reduced energy spread and emittance) is demonstrated in Fig. 6. In left plot in Fig. 6 note as the deviation of the electron beam off the axis ~10 μm

on one undulator length, which yields ~2μrad angle, potentially gives rise to the 2nd harmonic (orange surface) in hard X-rays. The deviation of the beam in the soft X-ray experiment in few undulator segments amounted to 20 μm on the undulator length [36]. This induces the angle 4 μm, which can not cause any measurable value for the 2nd harmonic (see right plot in Fig. 6) even in the case of the improved energy spread and divergence.

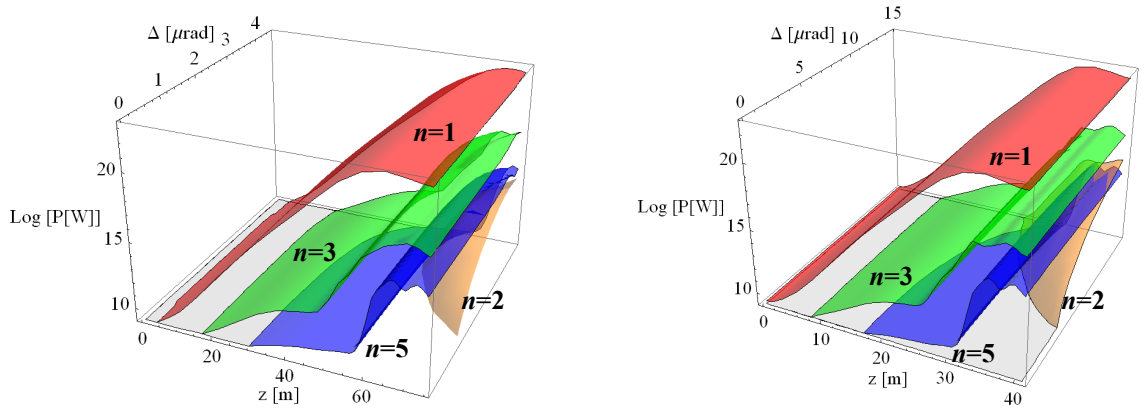

Fig. 6. Possible generation of high harmonics in POHANG FEL experiments (beam energy spread and emittances are assumed to allow high harmonic generation): right plot — soft X-rays, λ_1=1.52 nm and left plot — hard X-rays, λ_1=0.144 nm. The harmonics are color coded: *n*=1 — red surface, *n*=2 — orange surface, *n*=3 — green surface, *n*=5 — blue surface.

Eventually, let us estimate the spectral line split and width in PAL-XFEL experiments. Omitting the details, we note that in soft X-rays the spectral line is split in p=0,±1,±2,±3,±4 subharmonics (see Fig. 7); higher subharmonics are negligible. The fundamental line λ_1=1.5 nm is split in 9 subharmonics; its total width is small: $\Delta\lambda\sim 2.3$ pm, the relative value is $\Delta\lambda/\lambda\sim 1.5\times10^{-3}$. The latter value is small, but it is higher than the respective value in the soft X-ray LCLS experiment, where $\Delta\lambda/\lambda\sim 5\times10^{-4}$. For hard X-rays in PAL-XFEL we have to account for more subharmonics: p=0,±1,±2,±3,±4,±5,±6,±7. Their contribution is non-indifferent, although due to the ultrarelativistic electrons the line remains altogether narrow. We account for p=0,±1,±2,±3,±4,±5,±6,±7 subharmonics (see Fig. 8) and get the absolute value $\Delta\lambda\sim 0.14$ pm and small relative width $\Delta\lambda/\lambda\approx 1.0\times10^{-3}$. These values, being small, though exceed significantly the respective values in the LCLS experiment, where $\Delta\lambda/\lambda\approx 3\times10^{-5}$. The difference is in almost 1–2 orders of magnitude.

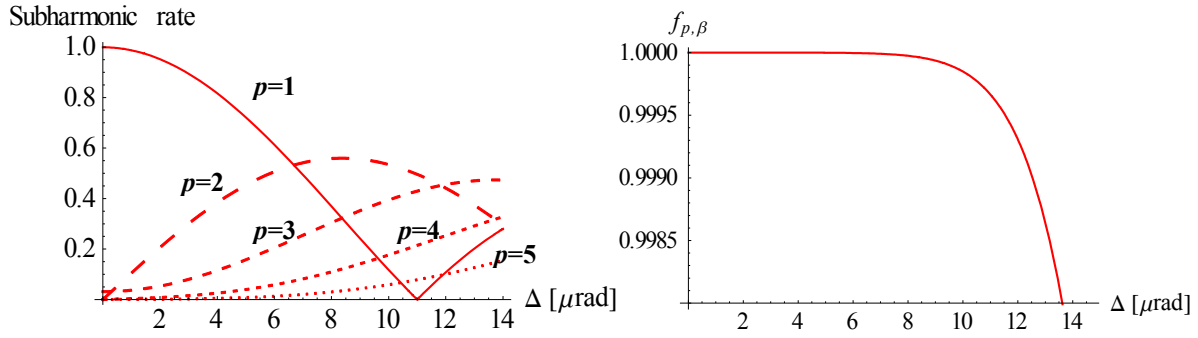

Fig. 7. Rate of subharmonics in the harmonic split of the line for soft X-ray POHANG experiment — left plot and total contribution rate of all subharmonic with $p\in[-4,+4]$ to the spectrum line for the angle Δ — right plot.

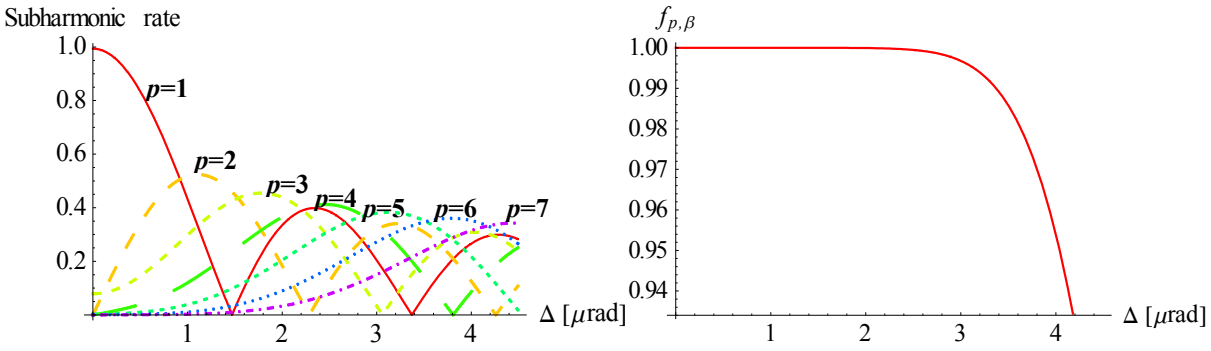

Fig. 8. Rate of subharmonics in the harmonic split of the line for hard X-ray POHANG experiment — left plot and total contribution rate of all subharmonic with $p \in [-7,+7]$ to the spectrum line for the angle Δ — right plot.

5. Results and conclusions

The analytical formalism for the study of free electron lasers radiation spectrums is presented, which accounts for all relevant loss factors in real installations and describes FEL harmonic power evolution. The obtained analytical expressions describe precisely FEL radiation spectrums in all bands. The comparison with a number of FEL experiments conducted in the last 2 decades in the range of radiated wavelengths from visible light to hard X-rays, confirms the validity of our analysis. The latter accounts explicitly for the finite beam size and off-axis position of electrons in it, the beam angular divergences, the electron energy spread, the non-periodic magnetic components and the undulator field harmonics. These factors are involved in the integral expressions for the generalized Bessel and Airy functions, which describe the spectral lines and their shapes as well as the effective split of the radiated FEL lines. The advantage of the formalism against commonly used 3-D numerical simulations consists in the possibility to separate and analyze contributions of each loss factor immediately. Thus allows deep insight into the underlying physical reasons for the radiation of selected FEL harmonics in each FEL with account for its specificity. We have performed the harmonic analysis in a number of FEL experiments and obtained perfect agreement with the measured results in every case.

We have modeled the FEL radiation in LCLS, LEUTL and POHANG installations for various instances of the conducted experiments with different from each other sets of parameters (see [20]–[24] and [36]). In particular, high harmonic generation in soft and hard X-ray bands was explored in the LCLS FEL experiments with the fundamental wavelengths λ_1=1.5 nm and λ_1=0.15 nm; high harmonic generation in UV–A band was explored in LEUTL FEL experiment with the fundamental wavelength λ_1=530 nm in visible band. In both experiments strong second harmonics were detected. Our modeling with account for the installation particularities is each experiment reproduces the measured values for the odd and even harmonic powers along the FEL undulators and agrees with the experimental data as shown in Fig. 3, Fig. 4. Employing the analytical formulae for the harmonic Bessel coefficients, we have distinguished and analyzed the contributions from the off-axis positions of the electrons in the beam, the divergence angle, the electron-phonon interaction angle on one gain length for each FEL harmonic with account for the beam energy spread and other parameters in each experiment. Our study demonstrates that significant radiation line split occurs in the experiments due to the finite beam size. However, high relativistic factors γ result in fine splits $\delta\lambda/\lambda \sim 1/\gamma$ between the subharmonics within one line; the radiation of all these subharmonics interact constructively with the electrons, grouping them. We have shown that betatron oscillations have very little effect on the power of even and odd FEL harmonics — it was practically negligible in all the considered cases; however, the calculated split of the spectrum lines due to the off-axis electrons position in the beam had noticeable values; they agreed with the experimental. Our analytical estimations for all FEL harmonics, such as the radiated powers, gain and saturation lengths, Pierce parameters and the spectrum line widths due to the split agree well the measured values.

We have shown that the off-axis position of the electrons in the LCLS FEL beam causes the split of the spectrum line; however, neither betatron oscillations nor the beam divergence can explain the measured power of the 2nd harmonic. Analytical computation demonstrated that it can be explained by the off-axis deviation of the electron beam in Δ~15 μm on the FEL gain length $L_g \approx 1.6$ m; it was detected and re-

ported in [20]–[22]. The resulting angular contributions give rise to the powerful 2nd harmonic and slightly attenuate the 3rd harmonic. The results of our analytical study agree well with those reported in [22].

We performed the detailed analysis of the radiation in the LEULT FEL experiment [23], [24] with the fundamental tone in the visible range, λ_1=580 nm, and in the UV–A range at λ_1=385 nm; both agree with our analytical results. In particular, the experiments with λ_1=580 nm were well documented, where high harmonic powers were carefully measured along the undulators and documented. They demonstrate upon the comparison (see Fig. 4) full agreement with our predictions. In the LEUTL experiments much bigger beam sizes $\sigma_{x.y}$~0.25 mm cause betatron oscillations, which split the spectrum line in roughly 5 subharmonics with the numbers p=0, ±1,±2. The resulting line width, ~6nm, perfectly agrees with the measured spectrum width, for example, of the second harmonic, Δλ~[266nm, 272nm] [23]. Our study shows that neither betatron oscillations, nor beam divergences could cause the 2nd harmonic of the measured power. We have demonstrated that the reason is in wide electron and photon beams, $\sigma_{x,y,\gamma}$ ~0.25–0.3 mm. This size matters for the photon-electron interaction on one gain length, L_g~1 m, and the effective angles $\gamma\bar{\theta} \approx 0.1$ arise in this wide beam. This causes the angular contribution, exceeding by 1–2 orders of magnitude that of the betatron oscillations and of the divergence and it gives rise to powerful 2nd FEL harmonic. With account for all above phenomena we get the harmonic power evolution within the range of the measured and estimated values, reported in [23], [24].

Moreover, we have analyzed the PAL-XFEL experiment at POHANG facility [36], where soft and hard X-rays were produced just like at the LCLS. Our analytical results are in good agreement with the reported values (see Fig. 5). The harmonics were not measured. We have modeled their possible behaviors in Fig. 6 with account for the beam sizes, divergences, electron-photon interaction angles, energy spread and diffraction; we concluded that the 2nd harmonic would be very weak due to small Pierce parameter, in particular, for hard X-rays. The spectral line in hard X-ray experiment is split in 15 subharmonics (see Fig. 8), despite that we get quite small width of the spectral line, $\Delta\lambda/\lambda \sim 1.0\times10^{-3}$, Δλ~0.14 pm due to γ~1500>>1. However, this line is ~30 times wider than that of the LCLS experiment at the same wavelength, where $\Delta\lambda/\lambda \approx 3\times10^{-5}$. The radiation of high harmonics at PAL-XFEL is limited by quite high energy spread: for hard X-rays $\sigma_e^{hard} = 0.00018$, the Pierce parameters are $\rho_1 \cong 0.0004, \rho_3 \cong 0.0002$, $\rho_5 \cong 0.00015$, $\rho_2 \cong 0.00006$; the energy spread for soft X-rays is $\sigma_e^{soft} = 0.0005$, and $\rho_1 \cong 0.0010, \rho_3 \cong 0.0006, \rho_5 \cong 0.0004, \rho_2 \cong 0.00007$. Based on that we can not expect the harmonics higher than the 3rd. We have suggested in Fig. 6 possible harmonic radiation at PAL-XFEL in the case the energy spread and emittance are improved.

The presented analytical formalism for FEL harmonic spectrum and power calculations yields the results, which agree with the measurements in wide range of wavelengths, from visible light to hard X-rays. The analytical formulae are relatively simple, do not require special computational environment and skills, and can be calculated on any PC or even engineering calculator. At the same time it is accurate and the predictions agree well the experimental values for each FEL experiment. Using this instrument we can estimate the performance, spectrum and harmonic power generation in planned and constructed FELs and conclude on the quality of the beams and their alignment in projected and currently operating FELs.

The authors are grateful to Prof. A.Borisov and Leading Researcher A.Lobanov for useful discussions.

6. Appendix: Phenomenological model for harmonic power evolution and gradual saturation in single-pass FEL

REFERENCES

[1] Ginzburg V.L., On the radiation of microradiowaves and their absorbtion in the air, *Isvestia Akademii Nauk SSSR (Fizika),* **11** N2 (1947) 1651.

[2] Motz H., Thon W., Whitehurst R.N.J., Experiments on radiation by fast electron beams, *Appl. Phys.,* **24** (1953)

826.

[3] McNeil B. W. J., Thompson N. R., X-ray free-electron lasers, *Nature Photonics*, **4** (2010) 814.

[4] Pellegrini C., Marinelli A., Reiche S., The physics of x-ray free-electron lasers, *Rev. Mod. Phys.,* **88** (2016), 015006.

[5] Schmüser P., Dohlus M., Rossbach J., Behrens C., *Free-Electron Lasers in the Ultraviolet and X-Ray Regime.* In: Springer Tracts in Modern Physics, **258**, Cham (ZG), Springer International Publishing. 2014.

[6] Huang Z., Kim K. J., Review of x-ray free-electron laser theory, *Phys.Rev. ST-AB*, **10**, 034801 (2007).

[7] Margaritondo G., Ribic P. R. A simplified description of x-ray free-electron lasers, *J. Synchrotron Rad.* **18,** 101 (2011).

[8] Saldin E. L., Schneidmiller E. A., Yurkov M. V., The Physics of Free Electron Lasers, Springer-Verlag Berlin Heidelberg, 2000.

[9] Bonifacio R., Pellegrini C., Narducci L., Collective instabilities and high-gain regime in a free electron laser, *Opt. Comm*., **50,** 373 (1984).

[10] Margaritondo, G., Synchrotron light: A success story over six decades, *Rivista del Nuovo Cimento*, **40** N9, 411 (2017).

[11] Bagrov V G, Bisnovaty-Kogan G S, Bordovitsyn V A, Borisov A V, Dorofeev O F, Ya Epp V, Pivovarov Y L, Shorokhov O V and Zhukovsky V C 1999 *Synchrotron Radiation Theory and Its Development* ed V A Bordovitsyn (Singapore: Word Scientific) p 447.

[12] Ternov I. M., Mikhailin V. V., Khalilov V. R., Synchrotron radiation and its applications. CRC Press, 1985.

[13] Margaritondo G. Characteristics and Properties of Synchrotron Radiation. In: Synchrotron Radiation. Mobilio S., Boscherini F., Meneghini C. (eds). Springer, Berlin, Heidelberg. 2015.

[14] Lee K., Mun J., Park S. Hee, Jang Kyu-Ha, Jeong Y., Vinokurov N.A., Numerical investigation of the radiation characteristics of a variable-period helical undulator*, Nucl. Instrum. Meth. Phys. Res. A* **776**, 27 (2015)

[15] Zhukovsky K., Kalitenko A., Phenomenological and numerical analysis of power evolution and bunching in single-pass X-ray FELs. Erratum, *J. Synchrotron Rad*. **26**, 605 (2019).

[16] Zhukovsky K., Analysis of harmonic generation in planar and elliptic bi-harmonic undulators and FELs, *Results in Physics*, **13,** 102248 (2019).

[17] Zhukovsky K.V., Effect of the 3rd undulator field harmonic on spontaneous and stimulated undulator radiation, *J. Synchrotron Rad*., **26,** 1481 (2019).

[18] Zhukovsky K.V., Generation of UR Harmonics in Undulators with Multiperiodic Fields, *Russian Physics Journal*, **62**, № 6, 1043-1053 (2019) .

[19] Alexeev V.I., Bessonov E.G., On some methods of generating circularly polarized hard undulator radiation, Nucl. *Instr. Meth. A* **308**, 140 (1991).

[20] Emma P., Akre R., Arthur J. *et al*., First lasing and operation of an angstrom-wavelength free-electron laser, *Nature, Photonics*, **4,** 641–647 (2010).

[21] Emma P., First lasing of the LCLS X-ray FEL at 1.5 Å, TH3PBI01, Proceedings of PAC09, Vancouver, BC, Canada, (2009).

[22] Ratner D., Brachmann A., Decker F.J. *et.al*., Second and third harmonic measurements at the linac coherent light source , *PhysRev ST-AB* **14**, 060701 (2011).

[23] S.G. Biedron et al., Measurements of nonlinear harmonic generation at the Advanced Photon Source's SASE FEL , *Nucl. Instrum. Meth. Phys. Res.* A 483 (2002) 94–100.

[24] S.V.Milton *et.al.*, Exponential Gain and Saturation of a Self-AmpliÞed Spontaneous Emission Free-Electron Laser, *Science* **292**, 2037–2041 (2000).

[25] Dattoli G., Ottaviani P. L., Pagnutti S., Nonlinear harmonic generation in high-gain free-electron lasers, *J. Appl. Phys*., **97** (2005) 113102.

[26] De Martini, F., 1990, in Laser Handbook, Vol. 6, edited by W. B. Colson, C. Pellegrini, and A. Renieri (North-Holland, Amsterdam), p.195.

[27] Bonifacio, R., De Salvo L., Pierini P., Large harmonic bunching in a high-gain free-electron laser, *Nucl. Instrum*. A, **293** (1990) 627.

[28] Huang Z., Kim K.-J., Three-dimensional analysis of harmonic generation in high-gain free-electron lasers, *Phys. Rev. E*, **62** (2000) 7295.

[29] Schneidmiller, E. A., Yurkov M. V., Harmonic lasing in x-ray free electron lasers, *Phys. Rev. ST*-AB, **15** (2012) 080702.

[30] McNeil, B.W. J., Robb G. R. M., Poole M.W. and Thompson N. R., Harmonic lasing in a free-electron-laser amplifier, *Phys. Rev. Lett*., **96** (2006) 084801.

[31] Yu L.-H., et.al., High-Gain Harmonic-Generation Free-Electron Laser, *Science*, 289 (2000) 932.

[32] Shaftan T., Yu L.-H., High-gain harmonic generation free-electron laser with variable wavelength, *Phys. Rev. E* 71, (2005) 046501.

[33] Zhukovsky K., Compact single-pass X-ray FEL with harmonic multiplication cascades, *Opt. Comm*. **418** (2018) 57–64.

[34] Zhukovsky K., Generation of coherent soft X-ray radiation in short FEL with harmonic multiplication cascades and two-frequency undulator, *J.Appl.Phy*s., **122** (2017) 233103.

[35] Zhukovsky K., Soft X-ray generation in cascade SASE FEL with two-frequency undulator, *EPL*, **119** (2017) 34002.

[36] Heung-Sik Kang *et.al.*, Hard X-ray free-electron laser with femtosecondscale timing jitter, *Nature Photonics*, **11** (2017) 708–713.

[37] Freund H.P., van der Slot P.J.M., Grimminck D.L.A.G., Setija I.D., Falgari P., Three-dimensional, time-dependent simulation of free-electron lasers with planar, helical, and elliptical undulators, *New J. Phys*. **19,** 023020 (2017).

[38] Henderson J.R., Campbell L.T., Freund H.P., McNeil B.W.J., *New J. Phys*. **18,** 062003 (2016).

[39] Freund, H. P., P. J. M. Van der Slot, Studies of a terawatt x-ray free-electron laser, *New J. Phys* , **20** N7, 073017 (2018).

[40] Zhukovsky K., Kalitenko A., Phenomenological and numerical analysis of power evolution and bunching in single-pass X-ray FELs, *J. Synchrotron Rad*., **26**, (2019) 159–169.

[41] Zhukovsky K., Kalitenko A., Harmonic generation in planar undulators in single-pass free electron lasers, *Russian Physics Journal*, **62**, № 2 (2019) 354–362.

[42] K. Zhukovsky, Analytical account for a planar undulator performance in a constant magnetic field, *J. Electromagn. Waves Appl*, **28** N15 (2014) 1869–1887.

[43] Zhukovsky K.V., Harmonic Generation by Ultrarelativistic Electrons in a Planar Undulator and the Emission-Line Broadening, *J. Electromagn. Waves Appl*., **29** N1 (2015) 132–142.

[44] Dattoli G., Mikhailin V.V., Zhukovsky K., Undulator radiation in a periodic magnetic field with a constant component, *J. Appl. Phys*. **104** (2008) 124507.

[45] Dattoli G., Mikhailin V.V., Zhukovsky K.V., Mosc. Univ. Phys. Bull., **64** N5 (2009) 507–512.

[46] Bessonov, E. G., General and some particular solutions of the inverse problem of the particle radiation theory in external fields. *Nucl. Instr. Meth*. A, **282** (1989) 405–412.

[47] Bagrov, V. G., Zal'mezh, V. F., Nikitin, M. M., Epp, V. Y. Generation of a given linear polarized radiation in a plane undulator. *Nucl. Instr. Meth*. A, **261** (1987) 54-55.

[48] V.I. Alexeev, E.G. Bessonov, On some methods of generating circularly polarized hard undulator radiation, *Nucl. Instr. Meth*. A, **308**, (1991) 140.

[49] Zhukovsky K.V., Operational solution for some types of second order differential equations and for relevant physical problems, *J. Math. Anal. Appl*., **446** (2017) 628–647.

[50] Alferov D. F., Bashmakov Yu. A., Bessonov E. G., Ondulator radiation theory, *Zh. Tekh. Fiz*., 43, **10** (1973) 2126–2132 [*Sov. Phys.-Tech. Phys*., **18**, (1974) 1336].

[51] Alferov, D. F., Bashmakov, Y. A., Bessonov, E. G., Cherenkov, P. A., & Belovintsev, K. A. The ondulator as a source of electromagnetic radiation. *Part. Accel*., **9**, (1979) 223-236.

[52] Alferov, D. F., Yu A. Bashmakov, Cherenkov P. A., Radiation from relativistic electrons in a magnetic undulator, *Soviet Physics Uspekhi*, **32** N3 (1989) 200.

[53] Vinokurov, N. A., & Levichev, E. B., Undulators and wigglers for the production of radiation and other applications. *Physics-Uspekhi*, **58**, N9 (2015) 850.

[54] Bashmakov Y. A., Bessonov E. G., On certain features of particle radiation in natural undulators–crystals. *Radiation Effects*, **66**, (1982) 85–94.

[55] Dattoli G., Ottaviani P. L, Semi-analytical models of free electron laser saturation, *Opt.Comm.*, **204** N1 (2002) 283–297.

[56] Dattoli G., Giannessi, L., Ottaviani, P. L. and Ronsivalle C., Semi-analytical model of self-amplified spontaneous-emission free-electron lasers, including diffraction and pulse-propagation effects. *J. Appl. Phys*. **95** (2004). 3206–3210.

[57] Dattoli G., Ottaviani P. L., Pagnutti S., *Booklet for FEL design* (Frascati, Italy: ENEA Pubblicazioni) 2007.

[58] Prakash B., Huse V., Gehlot M., Mishra G., Mishra S., Analysis of spectral properties of harmonic undulator radiation of anelectromagnet undulator, *Optik*, **127** (2016) 1639.

[59] Zhukovskiy K.V., Kalitenko A.M., Comparative Analysis of Phenomenological and Numerical Modeling of Experiments with Single-Pass Free-Electron Lasers, *Radiaphys. Quantum Electronics*, **62**, № 1 (2019) 52–64.

[60] Zhukovsky K.V., Analytical Description of Nonlinear Harmonic Generation Close to the Saturation Region in Free Electron Lasers, *Mosc. Univ. Phys. Bull*., **74** № 5, 480–487 (2019).

[61] L. Giannessi *et al.,* Self-amplified spontaneous emission for a single pass free-electron laser, Phys. *Rev. ST-AB.*, **14** (2011) 060712.

[62] P. J. Neyman*, W. B. Colson, S. C. Gottshalk, A. M. M. Todd, *Free Electron Lasers in 2017*, 38th International Free Electron Laser Conference FEL2017, Santa Fe, NM, USA doi:10.18429/JACoW-FEL2017-MOP066.

[63] https://lightsources.org/lightsources-of-the-world/

Zhukovsky Konstantin, Professor Dr.Sc., e-mail: zhukovsk@physics.msu.ru.